MAGI2 antisense RNA 3 (MAGI2-AS3) knockdown contributes to prostate cancer by downregulating proline-rich membrane anchor 1 (PRIMA1) via miR-142-3p

Keywords
prostate cancer, MAGI2-AS3, malignant behavior

Abstract

Introduction

Long non-coding RNA Membrane-Associated Guanylate Kinase Inverted 2 Antisense RNA 3 (MAGI2-AS3) has been identified as a predictive characteristic for prostate cancer (PC). However, the underlying mechanism of MAGI2-AS3 in PC is yet unclear.

Material and methods

The gene expression was detected via reverse transcription quantitative PCR. Cell viability, apoptosis and invasion were detected via cell counting kit-8, caspase-3 activity, flow cytometry, and transwell assays. Tumor xenograft experiment was performed to measure the tumor growth in vivo. Luciferase and radioimmunoprecipitation assays were utilized to determine the association between microRNA (miR)-142-3p and MAGI2-AS3 or proline-rich membrane anchor 1 (PRIMA1).

Results

MAGI2-AS3 and PRIMA1 were established to be downregulated in PC, whereas miR-142-3p exhibited the upregulation in PC. In vitro and in vivo loss-of-function assays demonstrated that MAGI2-AS3 silencing increased the viability and invasiveness, enhanced the tumor growth of PC cells, while reducing apoptosis. PRIMA1 silencing in PC cells showed the similar effect as MAGI2-AS3 silencing. Moreover, the miR-142-3p inhibitor reversed the impacts of the downregulation of MAGI2-AS3 or PRIMA1 on the malignant behavior of PC cells.

Conclusions

MAGI2-AS3 knockdown enhanced the malignant behavior of PC cells by targeting miR-142-3p to suppress PRIMA1 expression. Our findings reveal that MAGI2-AS3 can be a promising therapeutic target for the treatment of PC.

MAGI2 antisense RNA 3 (MAGI2-AS3) knockdown contributes to prostate cancer by downregulating proline-rich membrane anchor 1 (PRIMA1) via miR-142-3p

Running title: MAGI2-AS3 knockdown promotes prostate cancer

Abstract

Background: Long non-coding RNA Membrane-Associated Guanylate Kinase Inverted 2 Antisense RNA 3 (MAGI2-AS3) has been identified as a predictive characteristic for prostate cancer (PC). However, the underlying mechanism of MAGI2-AS3 in PC is yet unclear.

Methos: The gene expression was detected via reverse transcription quantitative PCR. Cell viability, apoptosis and invasion were detected via cell counting kit-8, caspase-3 activity, flow cytometry, and transwell assays. Tumor xenograft experiment was performed to measure the tumor growth *in vivo*. Luciferase and radioimmunoprecipitation assays were utilized to determine the association between microRNA (miR)-142-3p and MAGI2-AS3 or proline-rich membrane anchor 1 (PRIMA1).

Results: MAGI2-AS3 and PRIMA1 were established to be downregulated in PC, whereas miR-142-3p exhibited the upregulation in PC. *In vitro and in vivo* loss-of-function assays demonstrated that MAGI2-AS3 silencing increased the viability and invasiveness, enhanced the tumor growth of PC cells, while reducing apoptosis. PRIMA1 silencing in PC cells showed the similar effect as MAGI2-AS3 silencing. Moreover, the miR-142-3p inhibitor reversed the impacts of the downregulation of MAGI2-AS3 or PRIMA1 on the malignant behavior of PC cells.

Conclusion: MAGI2-AS3 knockdown enhanced the malignant behavior of PC cells by targeting miR-142-3p to suppress PRIMA1 expression. Our findings reveal that MAGI2-AS3 can be a promising therapeutic target for the treatment of PC.

Key words: prostate cancer; malignant behavior; MAGI2-AS3

Highlights

- MAGI2-AS3 knockdown promotes PC progression.
- To control the expression of PRIMA1, MAGI2-AS3 sponged miR-142-3p.
- The effects of PRIMA1 may be countered by miR-142-3p on PC.

Introduction

Prostate cancer (PC) is a frequently diagnosed neoplasm originating in the male reproductive system, with 1.4 million new cases and more than 370,000 deaths reported globally [1, 2]. Patients with PC generally present no noticeable symptoms, which suggests that PC is usually diagnosed at an advanced stage. Current intensive multimodal therapies, including radical prostatectomy and radiotherapy, have improved the patient prognosis [3]; however, so far, no effective therapeutic strategies are available for patients with metastatic PC [4]. In addition to age, endogenous hormone balance and genetic (predisposing) factors also increase the disease burden [5]. Therefore, in order to find effective therapeutic and diagnostic targets for PC, knowing the underlying molecular process of PC is required.

Non-coding RNAs, a class of non-coding transcripts, were initially recognized as junk or inconsequential transcription; however, increasing evidence has revealed their biofunctions and mechanism of action [6]. Non-coding RNAs that are longer than 200 nucleotides are known as long non-coding RNAs (lncRNAs) [7, 8]. They are tissue- and disease-specific. LncRNAs coordinate the DNA, proteins, and RNAs, and actively participate in various modulation mechanisms, thereby governing gene expression and influencing various pathological states [9]. Notably, emerging evidence have indicated that lncRNAs may serve as a "sponge/decoy" of microRNAs (miRNAs), suppress their action, and reshape miRNA targeted genes expression [10]. So far, the functions of

lncRNAs in PC remain mostly uncharacterized. Cai et al. analyzed a public online database and described Membrane-Associated Guanylate Kinase Inverted 2 Antisense RNA 3 (MAGI2-AS3) as a prognostic biomarker for PC [11]. However, the underlying molecular mechanisms of MAGI2-AS3 on specific the development of PC cells remain unclear.

Proline-rich membrane anchor 1 (PRIMA1) is an organizer responsible for the acetylcholinesterase tetramer formation and is implicated in various catabolic processes of neurotransmitters. Previously, low PRIMA1 expression was detected in colorectal cancer [12]. Interestingly, PRIMA1 is recognized as a mutant p53 reactivator and rescues its tumor suppressor role in breast, colorectal, thyroid, and bladder cancers [13-16]. Treatment with the PRIMA1 reagent, specifically in PC, decreases PC cell growth and causes death via raising the expression of P53. Treatment with the PRIMA1 reagent, specifically in PC, decreases PC cell growth and causes death via raising the expression of P53 [16, 17]. All available evidence points to a potential function for PRIMA1 in cancer malignancy.

Herein, we first discovered that miR-142-3p coordinates with MAGI2-AS3 and PRIMA1 using bioinformatics analysis. Next, we examined their functional importance in PC *in vitro* and hypothesized that MAGI2-AS3 might be a promising target for PC by sponging miR-142-3p and releasing PRIMA1. Thus, the novel regulatory mechanism of MAGI2-AS3/miR-142-3p/PRIMA1 could be a promising therapeutic target for the treatment of PC.

Materials and methods

Clinical specimens

From PC patients who received their initial diagnosis at our institution, 34 pairs of samples of PC tissue and adjacent normal tissue (>3 cm from PC tissue) were taken. For later gene identification, the clinical tissues were kept at - 80 °C. The ethics committee of Xindu District People's Hospital of Chengdu granted its clearance (Approval number: 20190409). All patients provided their written, informed permission. The clinical information of 34 patients with PC has been listed in Table 1.

Cell culture and transfection

The American Type Culture Collection (ATCC, USA) provided normal human epithelial cells (RWPE1) and human prostate cancer cells (22RV1, DU145, and LNCap). RWPE1, 22RV1, and LNCap cells were cultivated in Roswell Park Memorial Institute-1640 medium (Gibco, USA). The minimal essential medium (Gibco, USA), which contains 10% fetal bovine serum (FBS) and 1% penicillin-streptomycin at 37 °C and 5% CO_2, was used to cultivate DU145 cells. miR-142-3p inhibitor, and their related controls (si-NC and inhibitor NC), small interfering RNAs (siRNAs) targeting MAGI2-AS3 as well as PRIMA1 (si-MAGI2-AS3 as well as si-PRIMA1), were obtained from GenScript (Nanjing, China). First, 22RV1 and DU145 cells were transfected with Lipofectamine 2000 transfection reagent (Thermo Fisher, USA). Cells (1×10^5) were seeded in a 48-well plate with 500 μL of antibiotic-free growth medium. The plasmid was diluted in 50 μL Opti-MEM and mixed with Lipofectamine 2000 at room temperature for 20 minutes once the cells had attained 70–90% confluency. Next, 100 μL of the complex were gently added to each well and stirred. The cells were then cultured for 48 hours at 37 °C in a CO_2 incubator. Reverse transcription-quantitative polymerase chain reaction, or RT-qPCR, was used to confirm the transfection's efficacy.

Reverse Transcription quantitative PCR (RT-qPCR)

Utilizing the TransZol Up Plus RNA Kit, total RNA was isolated from PC cells as well as tissues (TransGen Biotech, Beijing, China). In the ImProm-II Reverse Transcription System (Promega, USA), cDNA was generated employing oligo (dT)-or miRNA-specific stem-loop primers. Primers (1 μL), ddH_2O (9 μL), and RNA (2 μg) were added to RNase-free tubes, which were then promptly put on ice after being warmed for 5 min at 65 °C. Then, 1 μL reverse transcriptase, 1 μL RNase inhibitor, 2 μL dNTP mix (10 mM), and 4 μL 5 × reaction buffer was added to the tube, carefully combined, and incubated in a water bath at 37 °C for one hour. The tube was then deactivated for 5 minutes in a water bath at 70 °C. Real-time PCR was used to quantify the acquired cDNA using the ABI PRISM 7500 Sequence Detection System obtained from Applied BioSystems, USA. The PCR was conducted at 55 °C for 10 min, succeeded by 40 cycles of 95 °C for 30 s, 55-59 °C for 30 s, and 72 °C for 42 s. The $2^{-\Delta\Delta Ct}$ technique was used to examine the results [18] after normalization with GAPDH or U6. Table 2 provides a list of the primers utilized in this investigation.

Localization of nucleus and cytoplasm

DU145 and 22RV1 cells had their cytoplasmic and nuclear RNA extracted using a Nuclear and Cytoplasmic RNA Purification Kit from Norgen (Canada). RT-qPCR was used to quantify the cytoplasmic and nuclear MAGI2-AS3 expression levels. GAPDH/U6 was applied as the cytoplasmic/nuclear control [19].

Cell proliferation assay

By employing the cell counting kit-8 (CCK-8) assay, cell proliferation was assessed (Beyotime, China). The 22RV1 and DU145 cells (1×10^5) were plated in a 96-well plate. At 0, 24, 48, and 72 hours following the completion of the maintenance phase, 10 μL of CCK-8 reagent were added. With the use of a DG-3022A microplate reader, the plates

were read at 450 nm (Nanjing Huadong Electron Tube Factory, China) [20].

Caspase-3 activity detection

A caspase-3 activity kit (Boyotime, China) was used to evaluate casepase-3 activity of the transfected cells after 48 h-transfection. Cell lysate treatment caused the cells to lyse. After centrifugation, 50 μL of the supernatant was collected for caspase-3 detection with substrate peptides, Ac-DEVD-pNA [21].

Flow cytometry assay

The Annexin V-fluorescein isothiocyanate (FITC)/propidium iodide (PI) Apoptosis Detection Kit (640914, BioLegend, USA) was employed for the apoptosis assay. Cells were briefly centrifuged at 250 × g for five minutes, resuspended in PBS, and combined with 500 μL of binding buffer (RVBB-01; Biomiga, USA). Then, 5 μL of AnnexinV-FITC was supplemented and properly integrated, afterward add 5 μL of PI. The cells were examined using a CytoFLEX flow cytometer after being maintained at 25 °C and shielded from light for 10 min (Beckman Coulter, USA) [22].

Transwell invasion assay

The medium (100 μL) with 22RV1 and DU145 cells (5×10^5) was placed on the upper transwell insert pre-added Matrigel (Corning Life Sciences, USA). The prepared insert was positioned in the lower compartment containing the medium (500 μL). Non-invading cells were removed after 24 hours of culture, and the quantity of invasive cells was counted after staining with 0.1% crystal violet [23].

Tumor xenograft experiment

Six BALB/c nude mice (4-weeks-old) purchased from Charles River (China) were divided to si-lnc group and si-NC group (n=3 mice per group). The MAGI2-AS3 knockdown lentiviral vector (si-lnc, GenScript, China) and its negative control (si-NC,

China) were transfected into 22RV1 cells, and then the transfected cells were injected subcutaneously into mice to induce tumor growth *in vivo*. The tumor volume was measured at 4, 8, 12, 16, 20, and 24 days. At 24 days, the mice were euthanized in a CO_2 chamber before their tumors were removed. Finally, the extracted tumors were photographed and weighed. This animal experiment was authorized by the Ethics Committee of Xindu District People's Hospital of Chengdu (Approval number: 202101125).

Dual-luciferase reporter (DLR) assay

PRIMA1, MAGI2-AS3, and miR-142-potential 3p's binding sequences were determined. Dual-luciferase constructs carrying the wild-type or mutant fragments of MAGI2-AS3 or PRIMA1 3′-untranslated region (UTR) (pMIR-REPORT-MAGI2-AS3-WT, pMIR-REPORT-MAGI2-AS3-MUT, pMIR-REPORT-PRIMA13'UTR WT, pMIR-REPORT-PRIMA13'UTR MUT) were obtained from GenScript (Nanjing, China). The constructed luciferase vectors were delivered into 22RV1 and DU145 cells along with the miR-142-3p or NC inhibitor. Using a DLR (dual-luciferase reporter) system, the result was evaluated 48 hours after transfection [24].

RNA immunoprecipitation (RIP)

A Magna RIP RNA-Binding Protein Immunoprecipitation Kit (17-700; Millipore, USA) was employed to confirm the interaction among MAGI2-AS3 and miR-142-3p. For 30 minutes, 22RV1 and DU145 cells were treated with the RIP lysis buffer. Magnetic beads coated with 5 μg of anti-Ago2 or unconjugated control IgG were added to the cell lysate and allowed to sit in the RIP buffer for 4 hours at 4 °C. Before RNA isolation, the precipitate was collected and washed with PBS that had already been refrigerated. MAGI2-AS3 and miR-142-3p concentrations were measured via RT-qPCR analysisß

[25].

Western blotting

PC cells were treated with the RIPA buffer with an additional 5 min of ultrasonic treatment. The supernatant was collected after centrifugation in order to carry out the Bradford technique of concentration measurement. The material was put into a 10% sulfate-polyacrylamide gel for 20 microliters and electrophoresed for 30 minutes. The membranes were cultured with the anti-PRIMA1 (1:1000, Cat# ABIN3086296; Antibodies online lnc., USA) or anti-GAPDH (1:1000, Cat# MA1-16757; Thermofisher, USA) antibodies at 4 °C overnight following a 10-minute, room-temperature blocking process with 10% non-fat milk. At room temperature for 30 minutes, the secondary antibodies (HRP-conjugated, 1:1,000; Abcam, USA) were used to identify the bands. Visualization was performed using an ultra-high-sensitivity enhanced chemiluminescence kit (MedChemExpress, USA) [24].

Statistical analyses

In order to conduct the statistical analyses, GraphPad Prism 9.0 was used. The Shapiro-Wilk test was used to determine the normality of every dataset. Comparisons among two groups were performed applying Student's t-test. For multiple comparisons, analysis of variance was implemented. Correlations were examined using Pearson analysis. Statistical significance was set at $P < 0.05$.

Results

MAGI2-AS3 may regulate PC by upregulating PRIMA1 via miR-142-3p

Based on the data from the Gene Expression Profiling Interactive Analysis (GEPIA) database, MAGI2-AS3 was considerably downregulated in prostate adenocarcinoma

(Figure 1A). Seventy-one target miRNAs were predicted using the StarBase database. By intersecting the targets with the differentially-expressed genes (DEGs) of the GSE17317 and GSE34932 datasets, seven common miRNAs that were differentially expressed in PC and were also the targets of MAGI2-AS3 were identified (Figure 1B). Among the seven miRNAs, we noticed that the role of miR-142-3p was limited in PC [26]. Thus, we selected the MAGI2-AS3/miR-142-3p axis as focus of the study. By combining the DEGs from the GEPIA PRAD database with the targets of miR-142-3p, which were collected from StarBase, six shared genes were found: Iduronate 2-sulfatase, butyrophilin-like 9, dynein heavy chain domain 1, PRIMA1, and tubulointerstitial nephritis antigen like 1 are all related proteins (Figure 1C). PRIMA1 was found to be downregulated in prostate adenocarcinoma by GEPIA analysis (Figure 1D, [27]), suggesting its potential role in this disease. However, PRIMA1 role in PC has not yet been studied.

MAGI2-AS3 knockdown promotes PC cell proliferation and invasion

Considering the downregulation of MAGI2-AS3 based on the GEPIA database analysis, we further explored its role in PC cells. We first tested the expression levels MAGI2-AS3 in PC cells and tissues. Compared with normal prostate epithelial cell lines, MAGI2-AS3 expression was lesser in PC cells, especially in 22RV1 and DU145 cells (Figure 2A). Downregulated MAGI2-AS3 was detected in PC tissues (Figure 2B). We subsequently investigated the competing endogenous RNA (ceRNA) activity of MAGI2-AS3 due to its presence in the nucleus (Figure 2C). Following that, si-MAGI2-AS3 and NC were transfected into 22RV1 as well as DU145 cells in order to knock out MAGI2-AS3. As shown in Figure 2D and Supplementary Figure 1A, RT-qPCR confirmed the high silencing efficiency of MAGI2-AS3. The modification of cell phenotypes caused by MAGI2-AS3 silencing was then investigated in 22RV1 and DU145 cells. As shown in

Figure 2E, MAGI2-AS3 silencing caused a higher proliferative rate in both PC cell lines. Later casepase-3 activity and cell apoptosis monitoring revealed that the decreased MAGI2-AS3 expression was associated by decreased caspase-3 activity and cell appoptosis (Figure 2F and 2G). In addition, inhibition of endogenous MAGI2-AS3 expression also increased the invasiveness of PC cells (Figure 2H). These data suggest that downregulation of MAGI2-AS3 is responsible for the promotion of proliferation and invasion of PC cells.

MAGI2-AS3 knockdown promotes tumor growth *in vivo*

By tumor xenograft experiment, MAGI-AS3 knockdown was confirmed to be able to elevate the tumor volume (Figure 3A). After euthanizing mice and removing tumors, it could be seen that tumor size in MAGI-AS3 knockdown group was bigger than that in si-NC group (Figure 3B). Similarly, tumor weight in MAGI-AS3 knockdown group was heavier than that in si-NC group (Figure 3C). These results prove that silencing MAGI-AS3 could contribute to tumor growth *in vivo*.

Verification of the interplay between MAGI2-AS3 and miR-142-3p

We first used StarBase to predict binding interactions and found that miR-142-3p shared complementary sequences with MAGI2-AS3 (Figure 4A). Then, we generated the 22RV1 and DU145 cells using luciferase reporter vectors carrying MAGI2-AS3 (WT or MUT) with NC or miR-142-3p mimics. To find variations in the luciferase activity in PC cells, a luciferase activity test was carried out. Luciferase activity was significantly reduced in PC cells transfected with MAGI2-AS3 WT vectors and miR-142-3p mimics, while no changes were detected in other cell groups (Figure 4B). To validate whether MAGI2-AS3 indeed binds to miR-142-3p, Ago2-RIP assays were performed on both PC cell lines. In Figure 3C, significantly enriched miR-142-3p and MAGI2-AS3 were present in the anti-

Ago-2 groups. RT-qPCR analysis confirmed the upregulation of miR-142-3p in PC cells and tissues (Figure 4D and 4E). Further research revealed a substantial negative association among the expression levels of miR-142-3p and MAGI2-AS3 in PC tissues ($R^2 = 0.5705$, $p < 0.0001$) (Figure 4F). The Cancer Genome Atlas (TCGA) data shown a negative association among miR-142-3p and MAGI2-AS1 expression in PC (Supplementary Figure 2A). According to these findings, MAGI2-AS3 binds to miR-142-3p and has tumor-suppressive properties.

miR-142-3 inhibitor partially restores the functions of silenced MAGI2-AS3

Next, we examined the interplay between miR-142-3 and MAGI2-AS3 on cell behavior. We started by determining the levels of miR-142-3 expression in 22RV1 as well as DU145 cells. As depicted in Figure 5A and Supplementary Figure 1B, introduction of anti-miR-142-3 into PC cells resulted in prominently diminished miR-142-3 expression. Notably, miR-142-3 expression levels were significantly elevated in both PC cell lines upon MAGI2-AS3 silencing, which was rescued by an accompanying transfection of the miR-142-3 inhibitor. The reduced cell proliferation resulting from miR-142-3 inhibition was also recovered by MAGI2-AS3 silencing (Figure 5B). Similarly, the promotion of miR-142-3 inhibitory effects on caspase-3 activity and apoptosis rate were abrogated by the co-transfection of si-MAGI2-AS3 and anti-miR-142-3 in PC cells (Figure 5C and 5D). Additionally, the invasion rate of PC cells was significantly reduced when miR-142-3 expression was downregulated, and subsequently restored by co-transfection with si-MAGI2-AS3 (Figure 5E).

PRIMA1 is a target of miR-142-3p

As MAGI2-AS3 as well as miR-142-3p form a ceRNA regulation network, we further explored the downstream target ceRNA participants. StarBase database analysis focused

on PRIMA1 (Figure 6A). Previous reports have demonstrated the involvement of PRIMA1 in various cancers, including PC. When 22RV1 as well as DU145 cells were treated with miR-142-3p mimics, the PRIMA1-3′-UTR-WT-dependent luciferase activity was one-fold reduced, but the PRIMA1-3′-UTR-MUT-dependent activity was unaffected (Figure 6B). Furthermore, RT-qPCR analysis showed significant downregulation of PRIMA1 in PC tissues (Figure 6C). Poor PRIMA1 expression was also detected in 22RV1 and DU145 cells (Figure 6D). Intriguingly, miR-142-3p and PRIMA1 expression levels were shown to be inversely correlated in PC tissues (Figure 6E). TCGA data indicated an inverse correlation among miR-142-3p and PRIMA1 expression levels in PC (Supplementary Figure 2B). When combined, PRIMA1 may act as a target of miR-142-3p in PC.

In vitro suppression of PC cells by miR-142-3p inhibitors is restored after PRIMA1 silencing

We determined the transfection efficiency of si-PRIMA1 and found that PRIMA1 was stably knocked down (Supplementary Figure 1C). In addition, once si-PRIMA1 was transfected into PC cells, the expression of PRIMA1 protein was reduced, and miR-142-3p inhibitor induced the increase in PRIMA1 protein. Moreover, the transfection of miR-142-3p inhibitor restored the reduced PRIMA1 expression caused by si-PRIMA1 (Figure 7A). Next, we looked at how PC cells responded when the miR-142-3p inhibitor restored PRIMA1 expression in them. As shown in Figure 7B, a decrease in PRIMA1 expression increased the PC cell proliferation and rescued the reduced PC cell proliferation caused by anti-miR-142-3p treatment. The PRIMA1-silenced 22RV1 and DU145 cells had considerably lower caspase-3 activity and apoptosis rates, which were both restored by anti-miR-142-3p therapy, according to the results of the caspase-3 activity and flow

cytometry detection tests (Figure 7C and 7D). The addition of si-PRIMA1 abrogated the inhibitory impacts of the miR-142-3p inhibitor on PC cell invasion (Figure 7E). These data suggest that miR-142-3p-mediated PC cell malignancy is partially dependent on PRIMA1.

Discussion

PC is globally associated with high morbidity and fatality in humans [28]. Recent evidence has demonstrated that dysregulation of lncRNAs might be an important pathophysiological mechanism that enhances the predisposition to various cancers, including PC [29]; however, their biofunctions have not yet been fully characterized. We discovered that, in a miR-142-3p/PRIMA1-dependent way, MAGI2-AS3as a pro-tumor lncRNA to impair the proliferation and migration and raised caspase-3 activity of PC cells.

In accordance with the tissue it affects, MAGI2-AS3 either promotes or suppresses tumor growth in certain malignancies. For instance, a high concentration of MAGI2-AS3 favorably controls the cell migration as well as cell invasion of tumor in gastric cancer [30]. High levels of MAGI2-AS3 in cervical squamous cell carcinoma were associated with a poor prognosis for the condition [31]. In contrast, MAGI2-AS3 is badly expressed in hepatocellular carcinoma, and exogenous MAGI2-AS3 can clearly increase the malignant features of tumor cells [32, 33]. The anticancer function of MAGI2-AS3 in ovarian cancer has also been established [34]. Low levels of MAGI2-AS3 expression in PC tissues and cells were found in this investigation, which is also known in previous report [35, 36]. Also, the silencing of MAGI2-AS3 promoted PC cell proliferation as well as cell invasion and reduced caspase-3 activity.

LncRNAs actively participate in the control of diverse cell processes via various genetic mechanisms [37]. In particular, lncRNAs are widely accepted as endo-siRNAs of miRNA, which can lessen their regulatory effect on mRNAs with ceRNA activities [10]. This ceRNA regulatory network has previously been reported in PC. For example, Ding et al. [38] reported that the lncRNA Muscleblind Like Splicing Regulator 1 Antisense RNA 1 (MBNL1-AS1) inhibits the progression of PC by sponging miR-181a-5p and releasing the phosphatase and tensin homolog. Wu et al. [39] revealed that lncRNA Maternally Expressed 3 (MEG3) suppressed the malignant phenotype of PC by regulating the miR-9-5p/quaking-5 axis. Additionally, mounting data demonstrates that MAGI2-AS3 controls the amounts of miRNA and mRNA expression in many malignancies. By controlling the miR-3163/transmembrane protein 106B axis, MAGI2-AS3 promotes the growth of colorectal cancer [40]. MAGI2-AS3 competitively adsorbs miR-31-5p and upregulates tensin 1 levels, resulting in the remission of bladder cancer progression [41]. Malignant behavior in hepatocellular carcinoma is inhibited by the MAGI2-AS3/miR-374b-5p/SMG1 nonsense-mediated mRNA decay axis linked to the PI3K-related kinase (SMG1) [32]. Cytoplasmic distribution analysis showed increased MAGI2-AS3 levels in the cytoplasm, suggesting the presence of a MAGI2-AS3-modulating ceRNA network. Additionally, it is anticipated that miR-142-3p will serve as MAGI2-AS3's target in later tests and function as an onco miRNA in a variety of malignancies, including PC [26, 42]. Luciferase reporter and RNA RIP assays were used to validate this prediction. MAGI2-AS3 expression was negatively correlated with miR-142-3p expression in PC tissues. More importantly, the promotional effect of MAGI2-AS3 knockdown was restored by the additional transfection with anti-miR-142-3p. Our findings showed MAGI2-AS3 ceRNA activity in miR-142-3p.

P53 mutation is commonly observed in various cancers, including PC. PRIMA1 can reactivate p53 activity and inhibit cancer progression. Previously, PRIMA1 was reported to restore p53 activity and negatively govern PC cell fate. Congruently, we found that PRIMA1 silencing enhanced PC cell viability and invasion, while weakening the caspase-3 activity; however, its upstream regulatory mechanisms have not yet been elucidated in PC. We demonstrated that PRIMA1 shares binding pairs with miR-142-3p. In addition, poor PRIMA1 expression was observed in PC tissues and cells. Pearson's analysis showed an inverse correlation between PRIMA1 and miR-142-3p levels. si-PRIMA1 rescued the inhibitory impacts of anti-miR-142-3p treatment on the proliferation, invasion, and apoptosis of cells. Godfrey et al. found that miR-142-3p is downregulated in pancreatic ductal adenocarcinoma, and its overexpression can curb the invasive capacity of P53 mutant tumor cells [43], indicating that miR-142-3p might play different roles in a tissue-specific manner. Further studies should focus on the complex regulatory mechanisms involving miR-142-3p and p53.

A limitation of our study was the lack of clinical analysis. Future studies are necessary to investigate the correlation between the MAGI2-AS3/miR-142-3p/PRIMA axis and PC clinicopathology such as tumor stages, prognosis by collecting more clinical samples.

Conclusion

In this research, we discovered that MAGI2-AS3 silencing boosted PC cell proliferation, invasion, and tumor growth. Mechanistically, MAGI2-AS3 competitively bound to miR-142-3p, and MAGI2-AS3 knockdown enhanced the miR-142-3p expression. Then, the decreased miR-142-3p expression subsequently increased the expression of PRIMA1. In order to effectively treat PC, a therapeutic approach that targets the MAGI2-AS3/miR-

142-3p/PRIMA1 axis may be necessary.

Declarations

Acknowledgements

None.

Funding

There is no information about funding.

Conflicts of interest

The authors declare that they have no competing interests.

Ethics approval

The Xindu District People's Hospital of Chengdu's ethics committee gave its approval to the current study (Chengdu, China) (Approval number: 20190409). When handling clinical tissue samples, the ethical principles outlined in the Declaration of Helsinki are scrupulously adhered to. Each patient signed a written informed consent form.

This animal experiment was conducted in accordance with the ARRIVE guidelines and was authorized by the Ethics Committee of Xindu District People's Hospital of Chengdu.

Consent to participate

An informed consent document was signed by each patient.

Consent for publication

Participants gave their permission for their names to be published.

Data availability statement

For acceptable requests for the datasets used and/or analyzed during the current work, the relevant author will answer.

Code availability

Not available.

Authors' contributions

The tests were run, and the data analysis was done by WQL and XKH. The research was planned and designed by SDL and CYS. The data was acquired by CWL and QFT. Data processing and interpretation were handled using QFT. The article was reviewed and approved by all writers.

References

1. Wang G, Zhao D, Spring DJ, DePinho RA. Genetics and biology of prostate cancer. Genes & development. 2018;32(17-18):1105-40.
2. Grozescu T, Popa F. Prostate cancer between prognosis and adequate/proper therapy. Journal of medicine and life. 2017;10(1):5-12.
3. Komura K, Sweeney CJ, Inamoto T, Ibuki N, Azuma H, Kantoff PW. Current treatment strategies for advanced prostate cancer. International journal of urology : official journal of the Japanese Urological Association. 2018;25(3):220-31.
4. Rudnytsky PL. Winnicott and Freud. The Psychoanalytic study of the child. 1989;44:331-50.
5. Ferrís-i-Tortajada J, García-i-Castell J, Berbel-Tornero O, Ortega-García JA. [Constitutional risk factors in prostate cancer]. Actas urologicas espanolas. 2011;35(5):282-8.
6. Zhou B, Yang H, Yang C, Bao YL, Yang SM, Liu J, et al. Translation of noncoding RNAs and cancer. Cancer letters. 2021;497:89-99.
7. Renganathan A, Felley-Bosco E. Long Noncoding RNAs in Cancer and Therapeutic Potential. Advances in experimental medicine and biology. 2017;1008:199-222.
8. Choudhari R, Sedano MJ, Harrison AL, Subramani R, Lin KY, Ramos EI, et al. Long noncoding RNAs in cancer: From discovery to therapeutic targets. Advances in clinical chemistry. 2020;95:105-47.
9. Sarfi M, Abbastabar M, Khalili E. Long noncoding RNAs biomarker-based cancer assessment. Journal of cellular physiology. 2019;234(10):16971-86.
10. Paraskevopoulou MD, Hatzigeorgiou AG. Analyzing MiRNA-LncRNA Interactions. Methods in molecular biology (Clifton, NJ). 2016;1402:271-86.
11. Cai J, Chen Z, Chen X, Huang H, Lin X, Miao B. Coexpression Network Analysis Identifies a Novel Nine-RNA Signature to Improve Prognostic Prediction for Prostate Cancer Patients. BioMed research international. 2020;2020:4264291.
12. Kalmár A, Péterfia B, Hollósi P, Galamb O, Spisák S, Wichmann B, et al. DNA hypermethylation and decreased mRNA expression of MAL, PRIMA1, PTGDR and SFRP1 in colorectal adenoma and cancer. BMC cancer. 2015;15:736.
13. Kaur RP, Vasudeva K, Kumar R, Munshi A. Role of p53 Gene in Breast Cancer: Focus on Mutation Spectrum and Therapeutic Strategies. Current pharmaceutical design. 2018;24(30):3566-75.
14. Barták BK, Kalmár A, Péterfia B, Patai Á V, Galamb O, Valcz G, et al. Colorectal adenoma and cancer detection based on altered methylation pattern of SFRP1, SFRP2, SDC2, and PRIMA1 in plasma samples. Epigenetics. 2017;12(9):751-63.
15. Cui B, Yang Q, Guan H, Shi B, Hou P, Ji M. PRIMA-1, a mutant p53 reactivator, restores the sensitivity of TP53 mutant-type thyroid cancer cells to the histone methylation inhibitor 3-Deazaneplanocin A. The Journal of clinical endocrinology and metabolism. 2014;99(6):E962-70.
16. Piantino CB, Reis ST, Viana NI, Silva IA, Morais DR, Antunes AA, et al. Prima-1 induces apoptosis in bladder cancer cell lines by activating p53. Clinics (Sao Paulo, Brazil). 2013;68(3):297-303.
17. Zhang W, Yi B, Wang C, Chen D, Bae S, Wei S, et al. Silencing of CD24 Enhances the PRIMA-1-Induced Restoration of Mutant p53 in Prostate Cancer Cells. Clinical cancer research : an official journal of the American Association for Cancer Research. 2016;22(10):2545-54.
18. Livak KJ, Schmittgen TD. Analysis of relative gene expression data using real-time quantitative PCR and the 2(-Delta Delta C(T)) Method. Methods (San Diego, Calif). 2001;25(4):402-8.
19. Shi X, Huo J, Gao X, Cai H, Zhu W. A newly identified lncRNA H1FX-AS1 targets DACT1 to inhibit cervical cancer via sponging miR-324-3p. Cancer cell international. 2020;20:358.
20. Wu C, Wang Z, Tian X, Wang J, Zhang Y, Wu B. Long non-coding RNA DDX11-AS1 promotes esophageal carcinoma cell proliferation and migration through regulating the miR-514b-3p/RBX1 axis. Bioengineered. 2021;12(1):3772-86.
21. Liu ZF, Liang ZQ, Li L, Zhou YB, Wang ZB, Gu WF, et al. MiR-335 functions as a tumor suppressor and regulates survivin expression in osteosarcoma. European review for medical and pharmacological sciences. 2016;20(7):1251-7.
22. Han B, Ge Y, Cui J, Liu B. Down-regulation of lncRNA DNAJC3-AS1 inhibits colon cancer via regulating miR-214-3p/LIVIN axis. Bioengineered. 2020;11(1):524-35.
23. Zhang J, Zhang R, Ye Y. Long non-coding RNA (LncRNA) SNHG7/ Eukaryotic translation initiation

factor 4 gamma 2 (EIF4G2) involves in the malignant events of ovarian cancer cells with paclitaxel resistant. Bioengineered. 2021;12(2):10541-52.
24. Feng J, Li J, Qie P, Li Z, Xu Y, Tian Z. Long non-coding RNA (lncRNA) PGM5P4-AS1 inhibits lung cancer progression by up-regulating leucine zipper tumor suppressor (LZTS3) through sponging microRNA miR-1275. Bioengineered. 2021;12(1):196-207.
25. Liu Y, Zhao J, Zhang W, Gan J, Hu C, Huang G, et al. lncRNA GAS5 enhances G1 cell cycle arrest via binding to YBX1 to regulate p21 expression in stomach cancer. Scientific reports. 2015;5:10159.
26. Tan YF, Chen ZY, Wang L, Wang M, Liu XH. MiR-142-3p functions as an oncogene in prostate cancer by targeting FOXO1. Journal of Cancer. 2020;11(6):1614-24.
27. Vanaja DK, Ballman KV, Morlan BW, Cheville JC, Neumann RM, Lieber MM, et al. PDLIM4 repression by hypermethylation as a potential biomarker for prostate cancer. Clinical cancer research : an official journal of the American Association for Cancer Research. 2006;12(4):1128-36.
28. Ritch C, Cookson M. Recent trends in the management of advanced prostate cancer. F1000Research. 2018;7.
29. Lingadahalli S, Jadhao S, Sung YY, Chen M, Hu L, Chen X, et al. Novel lncRNA LINC00844 Regulates Prostate Cancer Cell Migration and Invasion through AR Signaling. Molecular cancer research : MCR. 2018;16(12):1865-78.
30. Liu K, Zhao D, Wang D. LINC00528 regulates myocardial infarction by targeting the miR-143-3p/COX-2 axis. Bioengineered. 2020;11(1):11-8.
31. Hou A, Zhang Y, Fan Y, Zheng Y, Zhou X, Liu H. LncRNA MAGI2-AS3 Affects Cell Invasion and Migration of Cervical Squamous Cell Carcinoma (CSCC) via Sponging miRNA-233/EPB41L3 Axis. Cancer management and research. 2020;12:4209-16.
32. Yin Z, Ma T, Yan J, Shi N, Zhang C, Lu X, et al. LncRNA MAGI2-AS3 inhibits hepatocellular carcinoma cell proliferation and migration by targeting the miR-374b-5p/SMG1 signaling pathway. Journal of cellular physiology. 2019;234(10):18825-36.
33. Fang G, Wang J, Sun X, Xu R, Zhao X, Shao L, et al. LncRNA MAGI2-AS3 is downregulated in the distant recurrence of hepatocellular carcinoma after surgical resection and affects migration and invasion via ROCK2. Annals of hepatology. 2020;19(5):535-40.
34. Chang H, Zhang X, Li B, Meng X. MAGI2-AS3 suppresses MYC signaling to inhibit cell proliferation and migration in ovarian cancer through targeting miR-525-5p/MXD1 axis. Cancer medicine. 2020;9(17):6377-86.
35. Hu R, Wu P, Liu J. LncRNA MAGI2-AS3 Inhibits Prostate Cancer Progression by Targeting the miR-142-3p. Hormone and metabolic research = Hormon- und Stoffwechselforschung = Hormones et metabolisme. 2022;54(11):754-9.
36. Wei X, Hou Y, Zhang Y, Zhang H, Sun Z, Meng X, et al. Long non-coding RNA MAGI2-AS3 inactivates STAT3 pathway to inhibit prostate cancer cell proliferation via acting as a microRNA-424-5p sponge. Journal of Cancer. 2022;13(1):343-53.
37. Peng WX, Koirala P, Mo YY. LncRNA-mediated regulation of cell signaling in cancer. Oncogene. 2017;36(41):5661-7.
38. Ding X, Xu X, He XF, Yuan Y, Chen C, Shen XY, et al. Muscleblind-like 1 antisense RNA 1 inhibits cell proliferation, invasion, and migration of prostate cancer by sponging miR-181a-5p and regulating PTEN/PI3K/AKT/mTOR signaling. Bioengineered. 2021;12(1):803-14.
39. Wu M, Huang Y, Chen T, Wang W, Yang S, Ye Z, et al. LncRNA MEG3 inhibits the progression of prostate cancer by modulating miR-9-5p/QKI-5 axis. Journal of cellular and molecular medicine. 2019;23(1):29-38.
40. Ren H, Li Z, Tang Z, Li J, Lang X. Long noncoding MAGI2-AS3 promotes colorectal cancer progression through regulating miR-3163/TMEM106B axis. Journal of cellular physiology. 2020;235(5):4824-33.
41. Tang C, Cai Y, Jiang H, Lv Z, Yang C, Xu H, et al. LncRNA MAGI2-AS3 inhibits bladder cancer progression by targeting the miR-31-5p/TNS1 axis. Aging. 2020;12(24):25547-63.
42. Liang L, Fu J, Wang S, Cen H, Zhang L, Mandukhail SR, et al. MiR-142-3p enhances chemosensitivity of breast cancer cells and inhibits autophagy by targeting HMGB1. Acta pharmaceutica Sinica B. 2020;10(6):1036-46.
43. Godfrey JD, Morton JP, Wilczynska A, Sansom OJ, Bushell MD. MiR-142-3p is downregulated in aggressive p53 mutant mouse models of pancreatic ductal adenocarcinoma by hypermethylation of its

locus. Cell death & disease. 2018;9(6):644.

Figure legends

Figure 1. MAGI2-AS3/miR-142-3p/PRIMA1 is selected as the study object.

A. MAGI2-AS3 expression in prostate adenocarcinoma (PRAD) as well as the normal control was analyzed by GEPIA. PRAD: prostate cancer. T: tumor; N: normal. PRAD, Prostate adenocarcinoma. B. The intersection between GSE17317 DEGs, GSE34932 DEGs and targets of MAGI2-AS3 predicted by starbase database. C. The intersection between the targets of miR-142-3p predicted by starbase and the DEGs in prostate cancer obtained from GEPIA database. D. The expression of PRIMA1 in prostate adenocarcinoma (PRAD) and the normal control was analyzed by GEPIA.

Figure 2. MAGI2-AS3 knockdown promotes PC cell proliferation and invasion.

A-B. MAGI2-AS3 expression was quantified by RT-qPCR in RWPE1, 22RV1, DU145 and LNCap cells (A) as well as the normal and PC tissues (B). C. The distribution of MAGI2-AS3 in 22RV1 as well as DU145 cells were ascertained via qRT-PCR. D. RT-qPCR examining si-NC as well as si-MAGI2-AS3 in addition to MAGI2-AS3 in 22RV1 as well as DU145 cells. E. Proliferation of 22RV1 and DU145 cells measured by CCK-8 assay. F. Casepase-3 activity measured by a casepase-3 kit. G. Cell apoptosis measured by flow cytometry. H. Transwell invasion test used to identify invasion of 22RV1 cells as well as DU145 cells. *P<0.05, **P<0.001 vs. the si-NC.

Figure 3. MAGI2-AS3 knockdown contributes to tumor growth in vivo.

A. The tumor volume was measured every 4 days. B. The images of the extracted tumor. C. The tumor weight of the extracted tumor. **P<0.001 vs. the si-NC.

Figure 4. MAGI2-AS3-interacting miR-142-3p is overexpressed in PC cells.

A. Target prediction for MAGI2-AS3 as well as miR-142-3p using starbase database. B. The association among miR-142-3p and MAGI2-AS3 in 22RV1 and DU145 cells was

determined by DLR assay, vs. miR-NC, **P<0.001; C. Binding of miR-142-3p and MAGI2-AS3 in both NP cells, assayed by RIP, followed by RT-qPCR, vs. Anti-lgG, **P<0.001; D. The expression of miR-142-3p in PC cells were tested via RT-qPCR vs. RWPE1, **P<0.001; E. The expression of miR-142-3p in PC tissues were tested with the help of RT-qPCR analysis. F. The correlation level among miR-142-3p and MAGI2-AS3 was determined.

Figure 5. Anti-miR-142-3 partially restores the function of MAGI2-AS3 inhibitor.

A. when si-NC, inhibitor-NC, inhibitor, si-NC, or si-lnc-inhibitor were transfected into DU145 and 22RV1 cells, respectively. Relative miR-142-3 expression was ascertained via RT-qPCR. B. The cell proliferation was analyzed by CCK-8. C. The casepase-3 activity was measured. D. Cell apoptosis measured by flow cytometry. E. The cell invasion was examined by Transwell invasion assay. $^{\#}$P<0.05, $^{\#\#}$P<0.001 vs. inhibitor-NC; *P<0.05, **P<0.001 vs. si-NC; §P<0.05, §§P<0.001 vs. si-lnc+inhibitor.

Figure 6. The targeted association between miR-142-3p and PRIMA1.

A. Starbase was used to predict the binding site of PRIMA1 shared with miR-142-3p. B. DLR assay was used to confirm that miR-142-3p and PRIMA1 interacted in 22RV1 and DU145 cells. **P<0.001 vs. miR-NC; C. RT-qPCR was used to identify the PRIMA1 mRNA expression in PC tissues and normal tissues in comparison to RWPE1, **P<0.001; D. By using RT-qPCR, the mRNA expression of PRIMA1 in PC cells was assessed. **P<0.001; E. PRIMA1 mRNA expression and miR-142-3p expression are inversely correlated in PC tissues.

Figure 7. PRIMA1 partially restores the effect of miR-142-3p.

A. Inhibitor-NC, miR-142-3p inhibitor, miR-142-3p inhibitor+siPRIMA1, or si-NC were each transfected into 22RV1 and DU145 cells separately. Additionally, a western blot

analysis was applied to assess the relative PRIMA1 protein level. B-D. By using CCK-8, caspase-3, and flow cytometry detection, the rate of cell division and casepase-3 activity were evaluated. E. After transfecting with inhibitor-NC, miR-142-3p inhibitor, miR-142-3p inhibitor + siPRIMA1, or si-NC, separately, the cell invasion was measured using the Transwell invasion test. $^{\#}P<0.05$, $^{\#\#}P<0.001$ vs. inhibitor-NC; *P<0.05, **P<0.001 vs. si-NC; $^{\S}P<0.05$, $^{\S\S}P<0.001$ vs. si-lnc+inhibitor.

Supplementary Figure 1. Transfection efficiency.

A. qRT-PCR was used to identify MAGI2-AS3 expression in 22RV1 and DU145 cells transfected with si-NC and si-lnc at 0, 24, and 72 hours after transfection. against. si-NC **P<0.001. B. The expression of miR-142-3p in 22RV1 and DU145 cells transfected with inhibitor-NC and miR-142-3p inhibitor were detected by qRT-PCR at 0, 24, 48 and 72h after transfection. vs. inhibitor-NC, **P<0.001. C. By using qRT-PCR at 0, 24, 48, and 72 hours after transfection, MAGI2-AS3 expression in DU145 as well as 22RV1cells with si-NC and siPRIMA1 transfection was identified. **P<0.001 vs. si-NC.

Supplementary Figure 2. The correlation between MAGI2-AS3, miR-142-3p and PRIMA1 in PC samples according to TCGA data.

A. The correlation between miR-142-3p and MAGI2-AS1 in PC. B. The relationship in PC among miR-142-3p and PRIMA1.

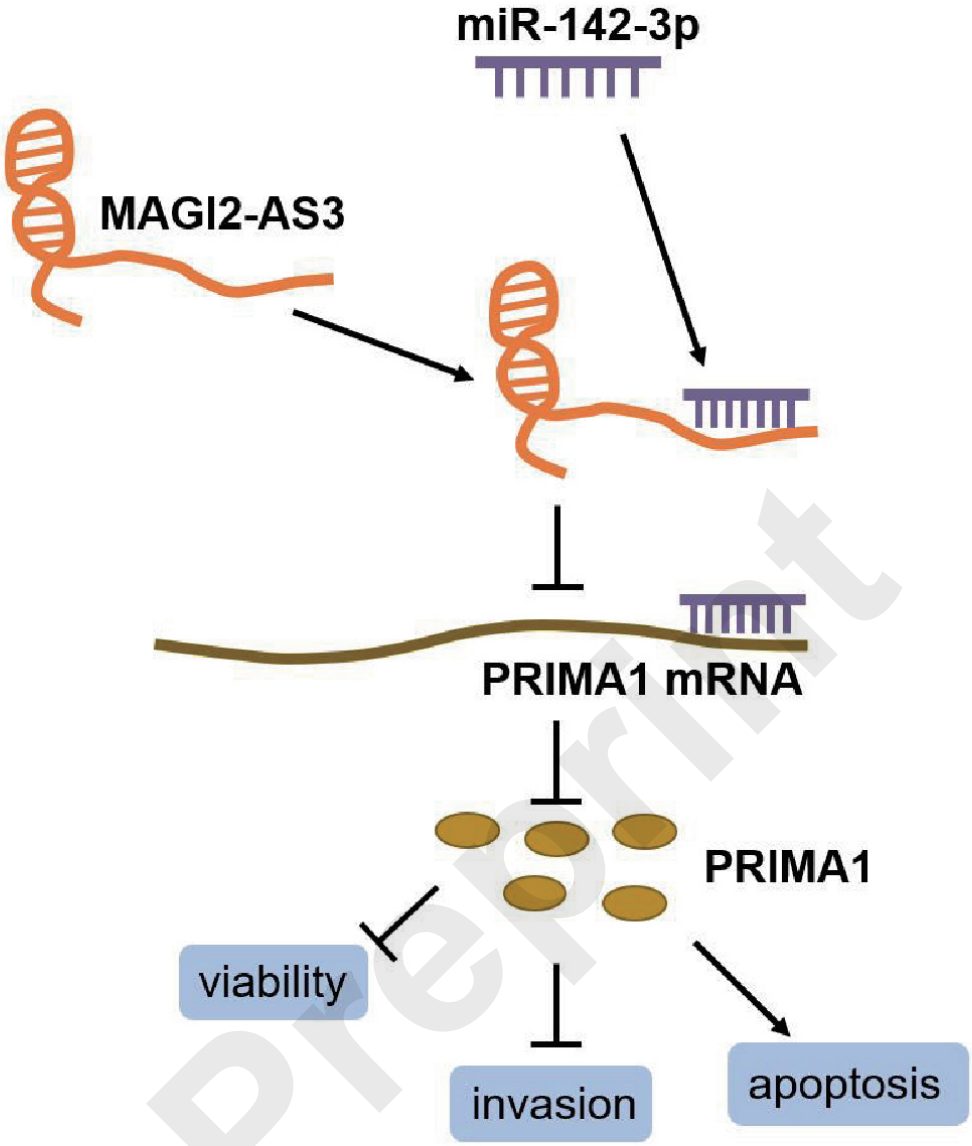
miR-142-3p
MAGI2-AS3
PRIMA1 mRNA
PRIMA1
viability
invasion
apoptosis

Table 1. Characteristics of 34 patients with PC.

Characteristic	Case
Age	
≤60	17
>60	17
Gleason Grade	
≤7	14
8-10	20
PSA (ng/mL)	
≤10	18
>10	16
Tumor stage	
T1-T2	15
T3-T4	19
Distant metastasis	
Yes	18
No	16

PSA, prostate-specific antigen.

Table 2 The primers used in the presence work

Targets	Primers	Sequences (5' to 3')
MAGI2-AS3	Forward	5’-CACCTTGCTTGA CAACTTGA-3’
	Reverse	5’-CATTACAGCTCGGCTACTGC-3’
miR-142-3p	Forward	5′-CTCCTGTAGTGTTTCCTAC-3′
	Reverse	5′-GACTGTTCCTCTCTTCCTC-3′
PRIMA1	Forward	5′-CTGCTCCAAAGTGACTGACAGC-3′
	Reverse	5′-GGGCAAGAGGTAGAGTTGGGAG-3′
U6	Forward	5′-CTCGCTTCGGCAGCACA-3′
	Reverse	5′-ACGCTTCACGAATTTGCGT-3′
GAPDH	Forward	5’-TGTAGTTGAGGTCAATGAAGGG-3’
	Reverse	5’-ACATCGCTCAGACACCATG-3’

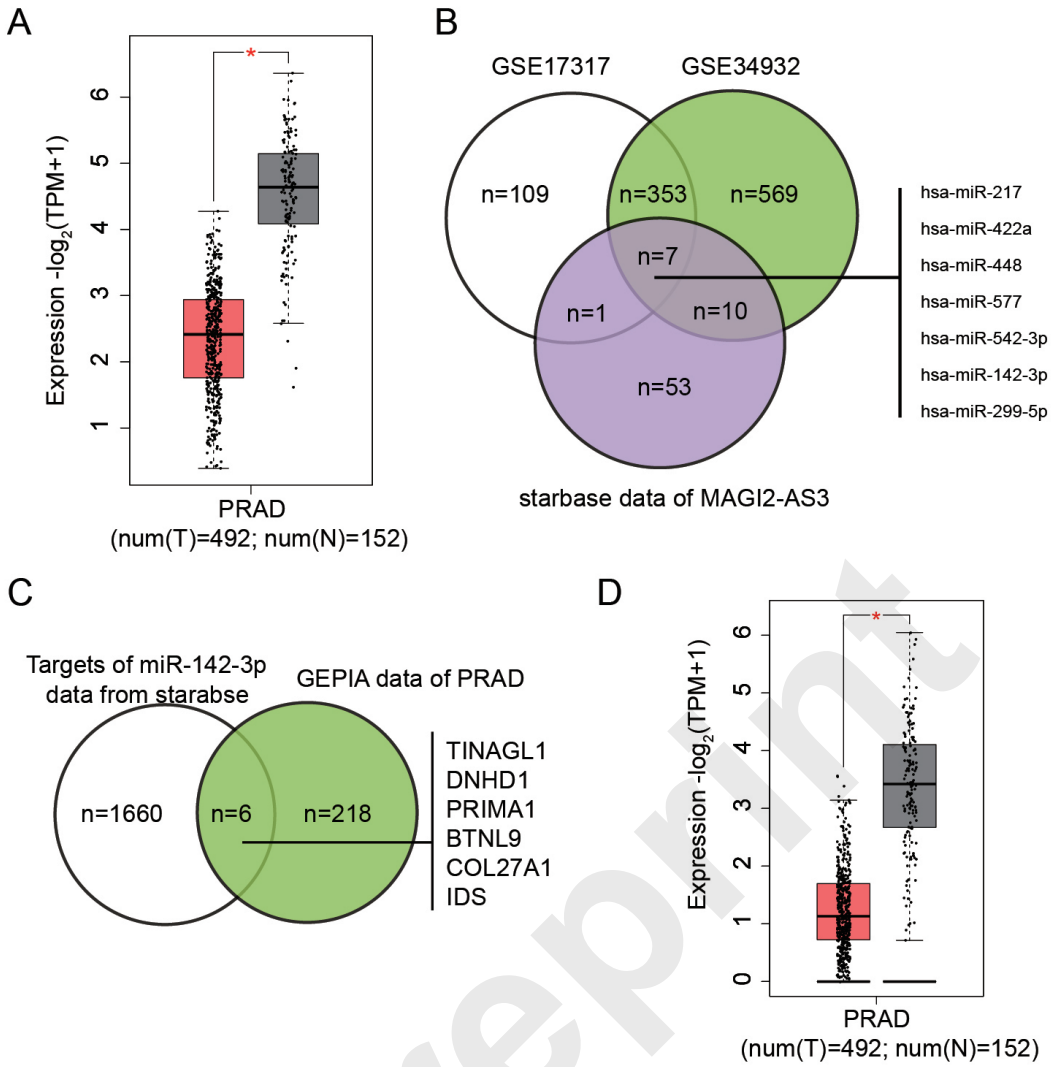

Figure 1. MAGI2-AS3/miR-142-3p/PRIMA1 is selected as the study object.
A. MAGI2-AS3 expression in prostate adenocarcinoma (PRAD) as well as the normal control was analyzed by GEPIA. PRAD: prostate cancer. T: tumor; N: normal. PRAD, Prostate adenocarcinoma. B. The intersection between GSE17317 DEGs, GSE34932 DEGs and targets of MAGI2-AS3 predicted by starbase database. C. The intersection between the targets of miR-142-3p predicted by starbase and the DEGs in prostate cancer obtained from GEPIA database. D. The expression of PRIMA1 in prostate adenocarcinoma (PRAD) and the normal control was analyzed by GEPIA.

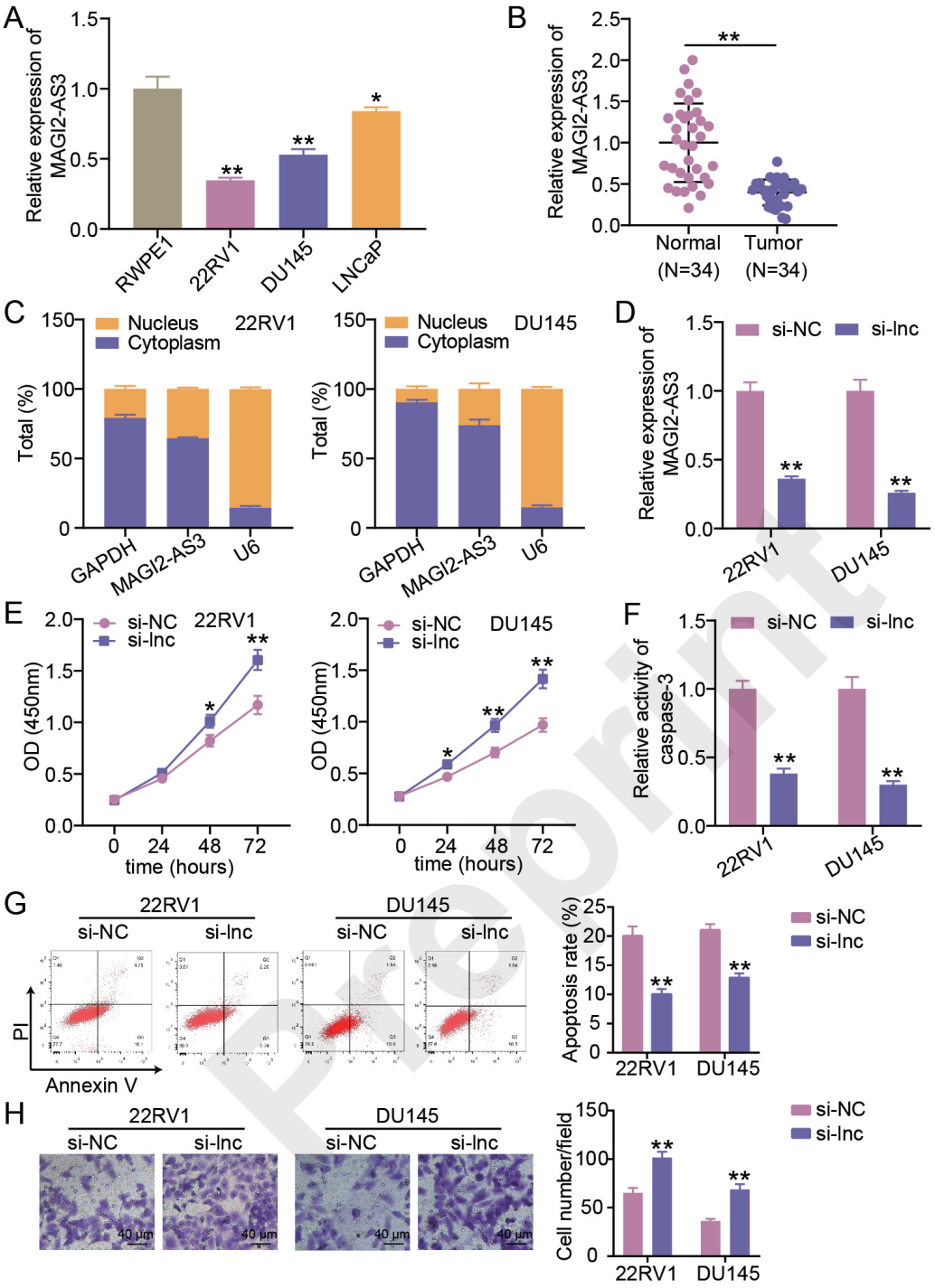

Figure 2. MAGI2-AS3 knockdown promotes PC cell proliferation and invasion.
A-B. MAGI2-AS3 expression was quantified by RT-qPCR in RWPE1, 22RV1, DU145 and LNCap cells (A) as well as the normal and PC tissues (B). C. The distribution of MAGI2-AS3 in 22RV1 as well as DU145 cells were ascertained via qRT□PCR. D. RT-qPCR examining si-NC as well as si-MAGI2-AS3 in addition to MAGI2-AS3 in 22RV1 as well as DU145 cells. E. Proliferation of 22RV1 and DU145 cells measured by CCK-8 assay. F. Casepase-3 activity measured by a casepase-3 kit. G. Cell apoptosis measured by flow cytometry. H. Transwell invasion test used to identify invasion of 22RV1 cells as well as DU145 cells. *P<0.05, **P<0.001 vs. the si□NC.

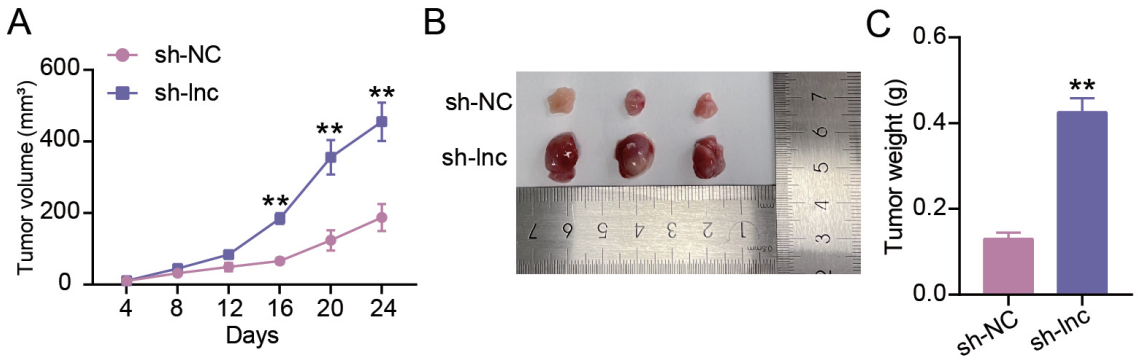

Figure 3. MAGI2-AS3 knockdown contributes to tumor growth in vivo.
A. The tumor volume was measured every 4 days. B. The images of the extracted tumor. C. The tumor weight of the extracted tumor. **P<0.001 vs. the si□NC.

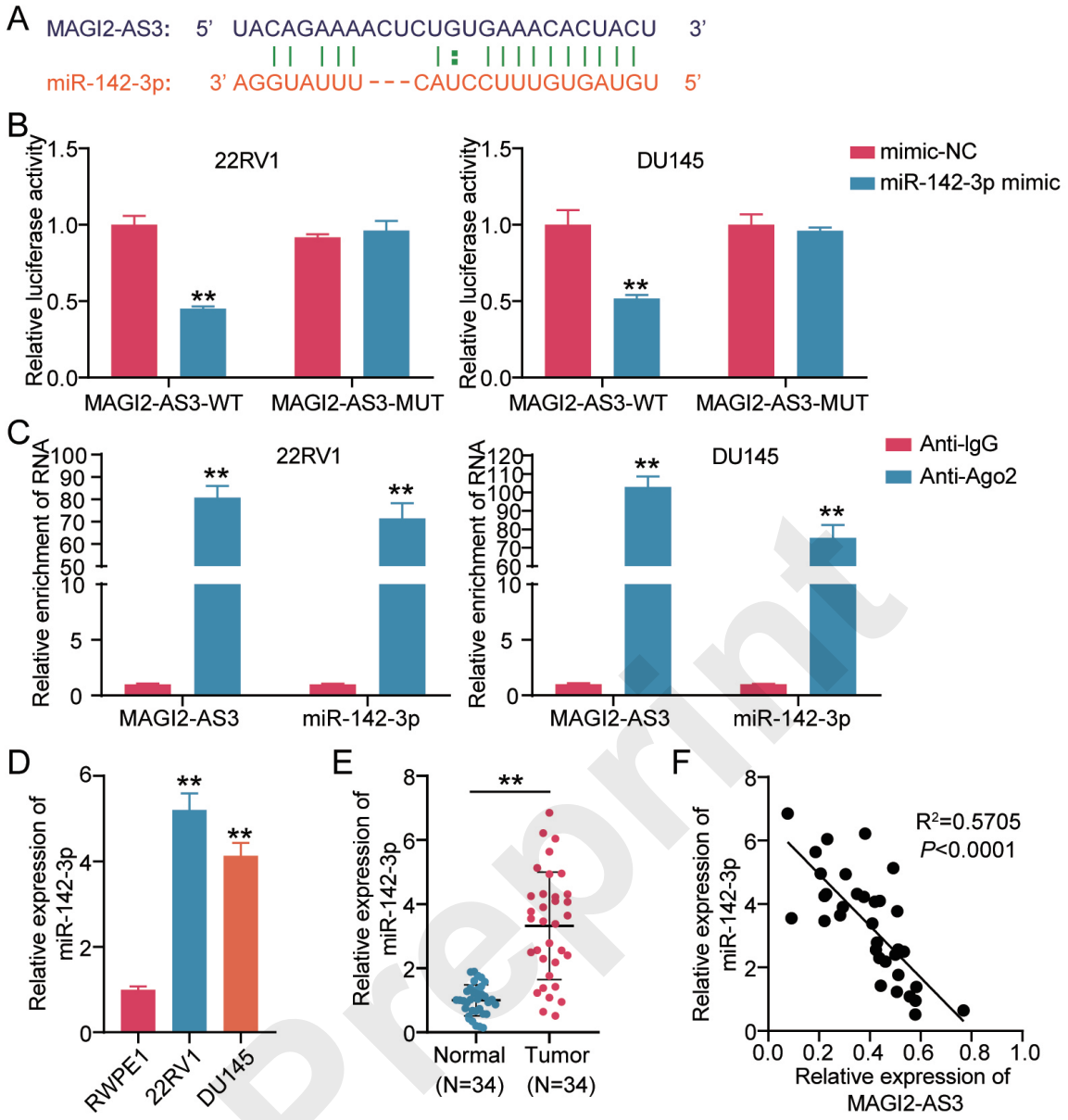

Figure 4. MAGI2-AS3-interacting miR-142-3p is overexpressed in PC cells.
A. Target prediction for MAGI2-AS3 as well as miR-142-3p using starbase database. B. The association among miR-142-3p and MAGI2-AS3 in 22RV1 and DU145 cells was determined by DLR assay, vs. miR-NC, **P<0.001; C. Binding of miR-142-3p and MAGI2-AS3 in both NP cells, assayed by RIP, followed by RT-qPCR, vs. Anti-IgG, **P<0.001; D. The expression of miR-142-3p in PC cells were tested via RT-qPCR vs. RWPE1, **P<0.001; E. The expression of miR-142-3p in PC tissues were tested with the help of RT-qPCR analysis. F. The correlation level among miR-142-3p and MAGI2-AS3 was determined.

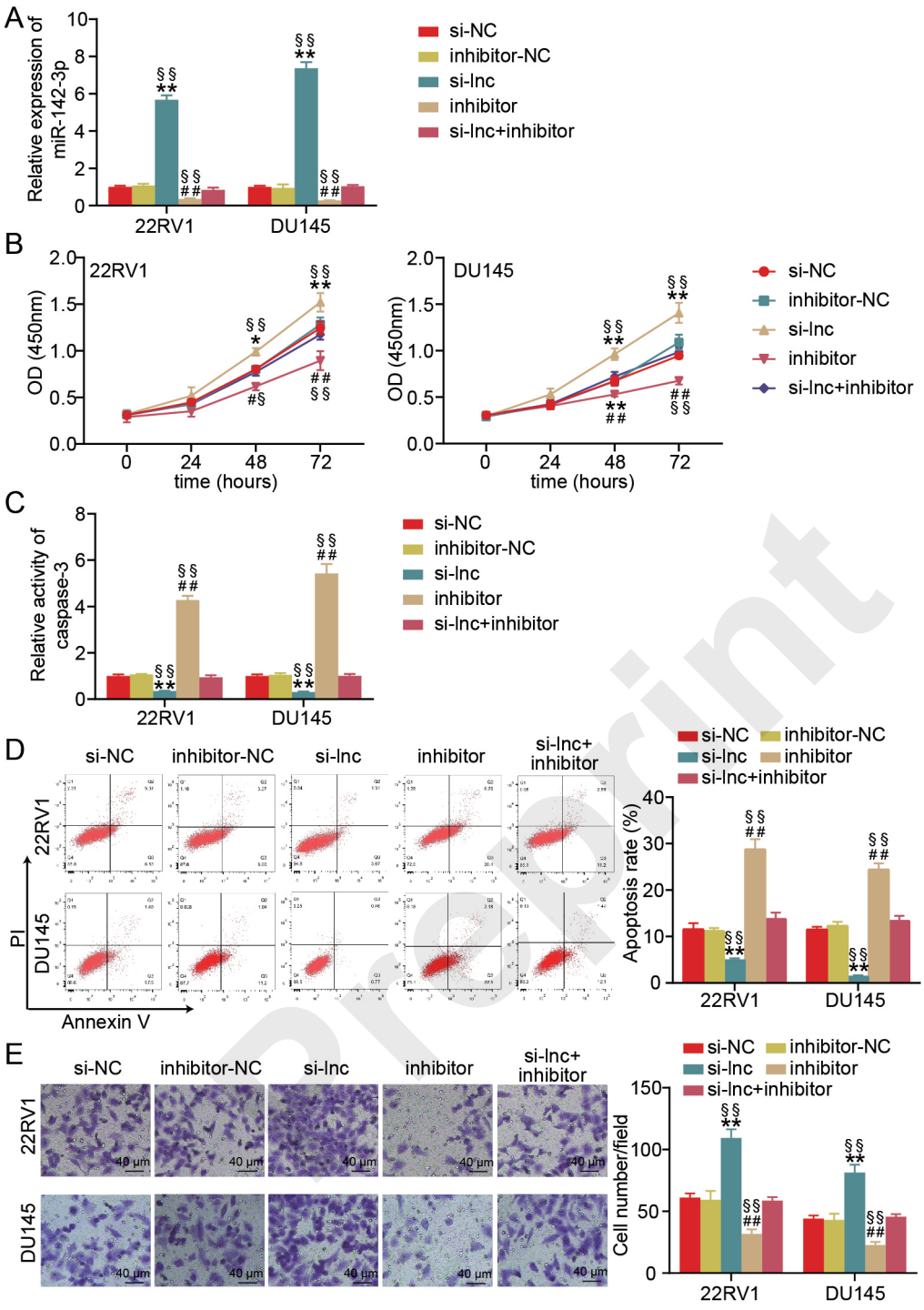

Figure 5. Anti-miR-142-3 partially restores the function of MAGI2-AS3 inhibitor.
A. when si-NC, inhibitor-NC, inhibitor, si-NC, or si-lnc-inhibitor were transfected into DU145 and 22RV1 cells, respectively. Relative miR-142-3 expression was ascertained via RT-qPCR. B. The cell proliferation was analyzed by CCK-8. C. The casepase-3 activity was measured. D. Cell apoptosis measured by flow cytometry. E. The cell invasion was examined by Transwell invasion assay. #P<0.05, ##P<0.001 vs. inhibitor-NC; *P<0.05, **P<0.001 vs. si-NC; §P<0.05, §§P<0.001 vs. si-lnc+inhibitor.

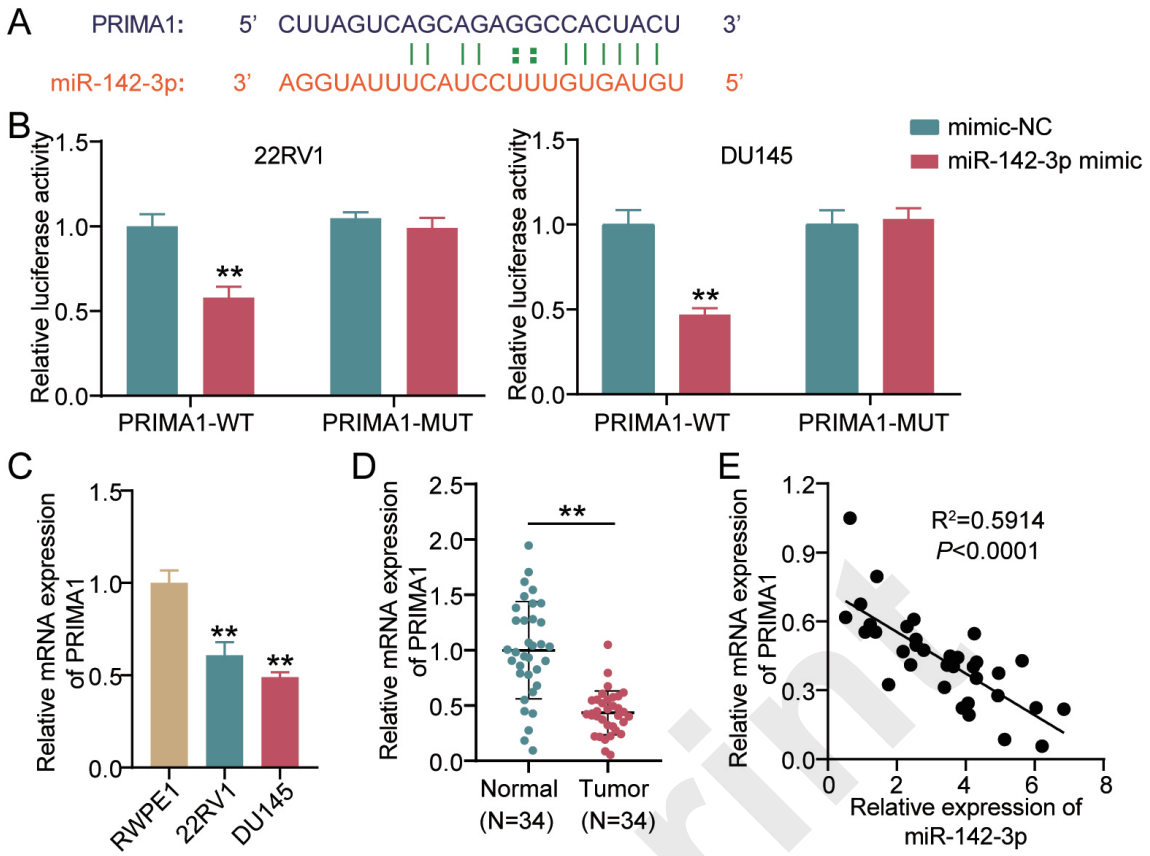

Figure 6. The targeted association between miR-142-3p and PRIMA1.
A. Starbase was used to predict the binding site of PRIMA1 shared with miR-142-3p. B. DLR assay was used to confirm that miR-142-3p and PRIMA1 interacted in 22RV1 and DU145 cells. **P<0.001 vs. miR-NC; C. RT-qPCR was used to identify the PRIMA1 mRNA expression in PC tissues and normal tissues in comparison to RWPE1, **P<0.001; D. By using RT-qPCR, the mRNA expression of PRIMA1 in PC cells was assessed. **P<0.001; E. PRIMA1 mRNA expression and miR-142-3p expression are inversely correlated in PC tissues.

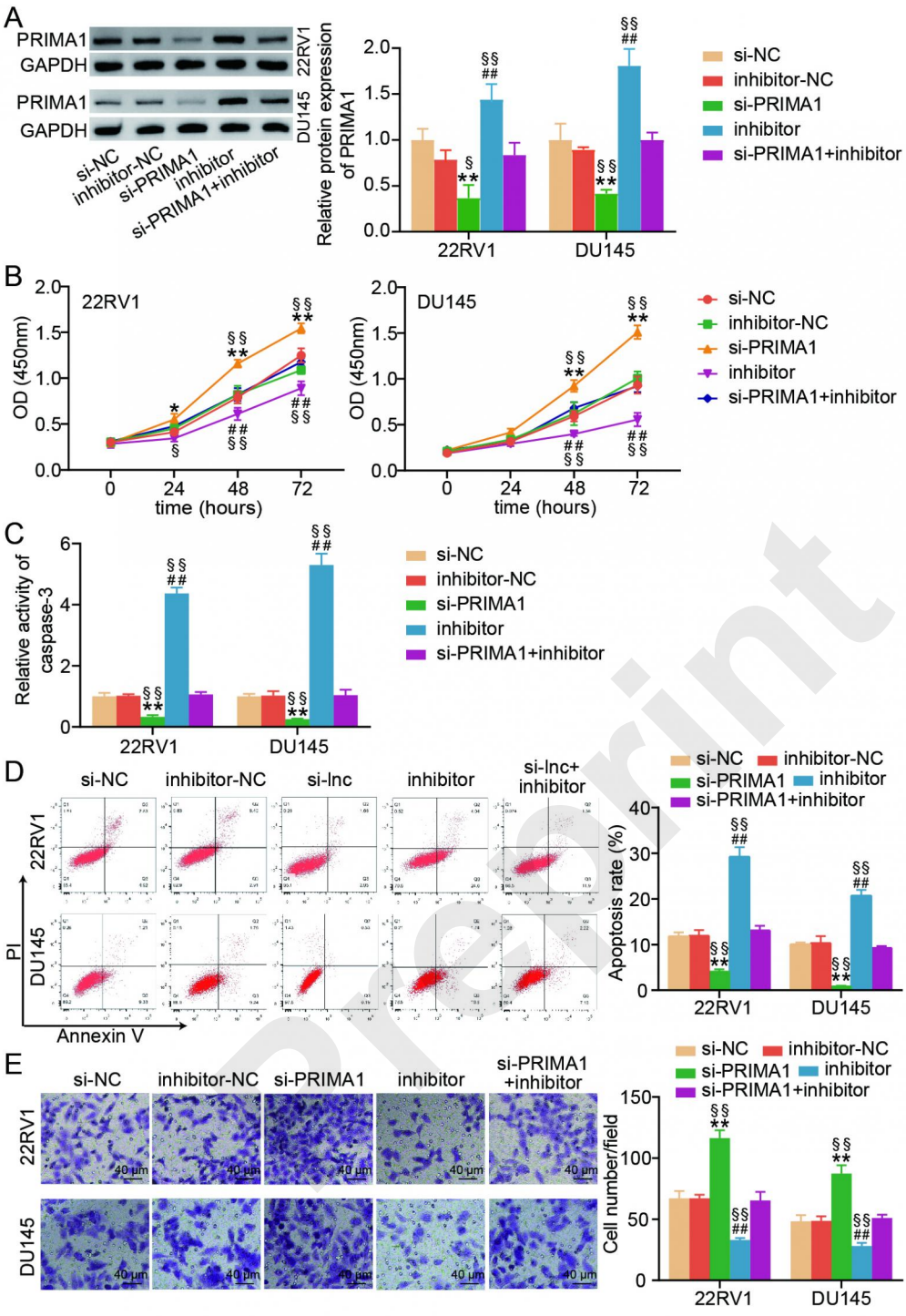

Figure 7. PRIMA1 partially restores the effect of miR-142-3p.
A. Inhibitor-NC, miR-142-3p inhibitor, miR-142-3p inhibitor+siPRIMA1, or si-NC were each transfected into 22RV1 and DU145 cells separately. Additionally, a western blot analysis was applied to assess the relative PRIMA1 protein level. B-D. By using CCK-8, caspase-3, and flow cytometry detection, the rate of cell division and casepase-3 activity were evaluated. E. After transfecting with inhibitor-NC, miR-142-3p inhibitor, miR-142-3p inhibitor + siPRIMA1, or si-NC, separately, the cell invasion was measured using the Transwell invasion test. #P<0.05, ##P<0.001 vs. inhibitor-NC; *P<0.05, **P<0.001 vs. si-NC; §P<0.05, §§P<0.001 vs. si-lnc+inhibitor.

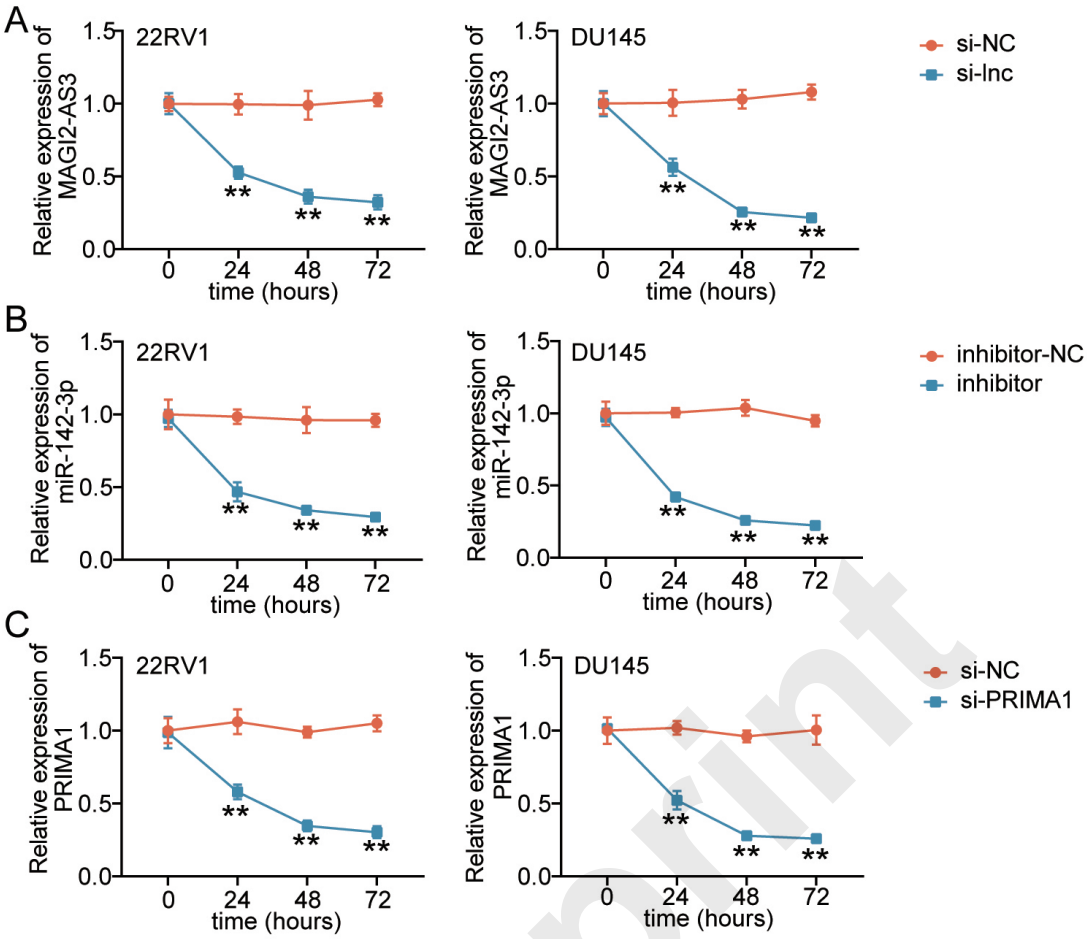

Supplementary Figure 1. Transfection efficiency.
A. qRT-PCR was used to identify MAGI2-AS3 expression in 22RV1 and DU145 cells transfected with si-NC and si-lnc at 0, 24, and 72 hours after transfection. against. si-NC **P<0.001. B. The expression of miR-142-3p in 22RV1 and DU145 cells transfected with inhibitor-NC and miR-142-3p inhibitor were detected by qRT□PCR at 0, 24, 48 and 72h after transfection. vs. inhibitor-NC, **P<0.001. C. By using qRT-PCR at 0, 24, 48, and 72 hours after transfection, MAGI2-AS3 expression in DU145 as well as 22RV1cells with si-NC and siPRIMA1 transfection was identified. **P<0.001 vs. si-NC.

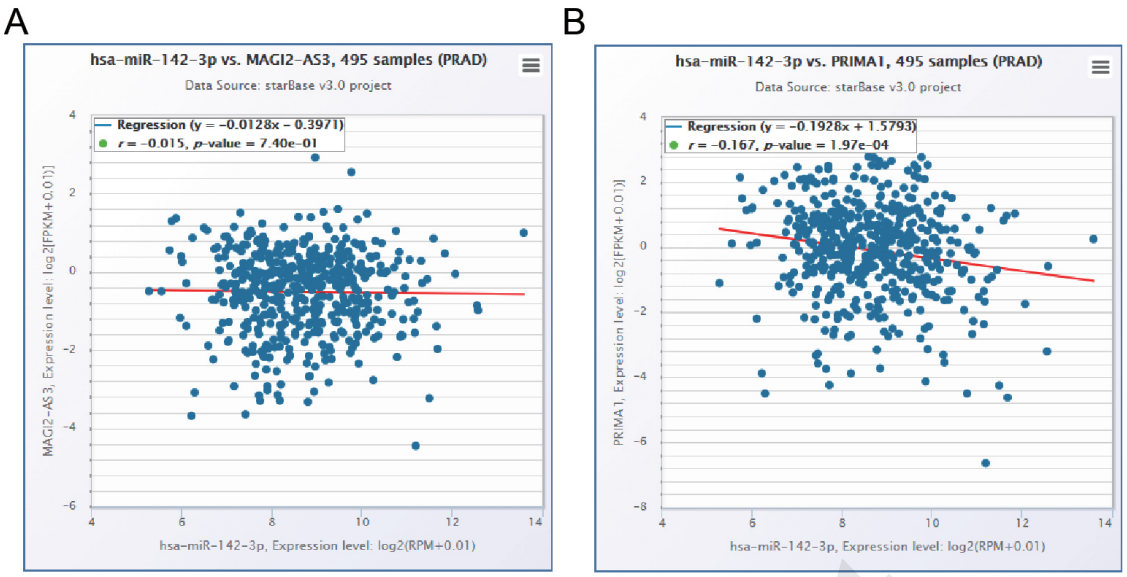

Supplementary Figure 2. The correlation between MAGI2-AS3, miR-142-3p and PRIMA1 in PC samples according to TCGA data.
A. The correlation between miR-142-3p and MAGI2-AS1 in PC. B. The relationship in PC among miR-142-3p and PRIMA1.